Fiber Bragg grating-based thermometer for drill bit temperature monitoring

Miguel Llera,[1,*] Kenny Hey Tow,[2] Sylvain Bergerat,[1] Yves Meyer,[1] Serge Monnerat,[1] Olivier Gloriod,[1] Sébastien Le Floch,[1] Yves Salvadé,[1] and Luc Thévenaz[2]

[1]Haute Ecole Arc Ingénierie, HES-SO, Rue de la Serre 7, 2610 Saint-Imier, Switzerland
[2]EPFL Swiss Federal Institute of Technology, Institute of Electrical Engineering, SCI STI LT, Station 11, CH-1015 Lausanne, Switzerland
*Corresponding author: Miguel.llera@he-arc.ch

The temperature measurement of a drill bit during an implantology drilling process is proposed by using a fiber Bragg grating fitted inside the drill bit. Due to the rotational nature of the drilling process, a free-space fiber-optic rotary joint is used for interrogating the fiber Bragg grating. Due to mechanical clearances and interferometric noise induced at this rotary joint, signal integrity is strongly deteriorated and is not workable without adequate measures. These measures involve a proper fiber lensing and a signal processing in order to remove the interferometric noise. Finally, a heating measurement on an implantology drill bit is performed and discussed for drilling several holes on a pork jaw sample. © 2019 Optical Society of America

1. INTRODUCTION

Drilling is a well-known process that generates heat due to the friction of the cutting tool with the material. For medical applications, as it is widely used in orthopedic surgery and dentistry, this warming can have a major implication. Bone drilling heating can cause osteonecrosis and it is believed that a common threshold of 47°C for a duration of 1 min [1] is the limit to not overcome in order to preserve bone properties. It is also known that the duration decreases exponentially with the temperature increase and for a temperature above 70°C an immediate damage is observed [2]. Drill bit specifications play an important role as how the drill bit will warm the bone during drilling [3,4].

Measuring the temperature at drilling sites is challenging because drill bits often rotate at high speeds (thousands of rpm) and heating is produced at the tool–bone interface. Tools to monitor temperature changes at a drilling point include thermocouples [5] and thermographic cameras [6]. Thermocouples have been extensively used but the poor thermal conductivity of the bones [7] and the need to drill pilot holes makes the technique unsatisfactory. Thermographic cameras have extensive applications in the medical field [8] and can be extremely helpful to get a temperature mapping of the detected area. Nevertheless, thermographic cameras measure the heat radiation emitted from a surface and are not able to directly measure the temperature inside a sample. Moreover, many standard constraints have to be followed in order to ensure reliable results [9], and the bulkiness of the camera itself and its instrumentation make the technique unsuitable for many drilling

procedures on a daily basis. Therefore, measuring directly the drill bit temperature would be the best option in order to avoid overheating of the bone. A first try involving the use of a non-rotary thermocouple inside the drill bit has been reported [10]. But this solution presents some drawbacks as thermocouples can wear due to unavoidable frictions within the rotating drill bit, and the drill bit structure can be weakened by the need of a central hole. However, frictions can only be avoided if the sensing element is inside the drill bit and rotates with it. Unfortunately, thermocouples are electrical components that cannot be used in a free-space coupling. An interesting technique that may be suitable for a free-space coupling is brought by the photonics world and more specifically by the fiber optic sensing [11].

Fiber optic sensing englobes many techniques that can bring solutions to many measurement challenges. Miniature fiber optic sensors are usually based on Fabry–Perot cavities along the fiber or at its tip [12], or fiber Bragg gratings (FBGs) [13]. Fabry–Perot cavities have the advantage to be extremely small, a few micrometers to several hundred micrometers cavities length, and then can be located in extreme locations [14] in order to perform remote monitoring of physical parameters. The sensing element in those configurations is the so-called diaphragm that plays the role of flexible outer mirror that can deflect by changing its physical conditions environment. Nevertheless, the diaphragms being extremely thin, typically less than a few micrometers, applications with strong vibrations will induce too much noise on the feedback signal, which makes it difficult to perform stable measurements. On the

other hand, FBGs can prove to be a more adapted solution. These gratings are manufactured by photoimprinting a refractive index periodic perturbation on the fiber core. The grating's reflected wavelength shifts with the perturbation's period and is hence thermal and strain dependent. Their solid and long configuration, usually a few millimeters to several centimeters, allows them to be more adapted for measuring physical conditions on vibrating elements. The FBG is a mature technology and the sensor and subsequent interrogation systems are readily available off-the-shelf at competitive prices.

However, interrogating a rotating FBG is not a trivial matter and brings additional challenges due to the poor expected signal-to-noise ratio (SNR). In this application, the FBG is inscribed on a fiber inserted in the rotating drill bit and a fixed lead fiber, going through the dental piece, will interrogate the rotating FBG. The free-space coupling between these two fibers needs to ensure a useful optical transmission despite the mechanical misalignments, brought by rotation, and interferometric noise added to the signal due to undesired reflections at the fiber–air interfaces. Free-space coupling interrogation of a rotary FBG have been mentioned in the literature [15–17] but none of these studies have reported about the impact of interferometric noise, induced by the fiber–air reflections, on the Bragg wavelength monitoring. Moreover, they make use of bulk commercial collimators, except for [16] where they couple lensless fibers in a capillary tube, that avoid any robust miniaturization of the rotary junction.

In this paper, we describe the interferometric noise induced on the Bragg wavelength spectrum and its mitigation by optical ways as well as by signal processing. Finally, based on previous work [18] we show and discuss the results of an application of FBG for monitoring drill bits temperature for bone drilling.

2. INTERFEROMETRIC NOISE

A. Noise Sources

Free-space coupling between the lead fiber and the FBG will generate reflective surfaces at the fiber tips. These reflective surfaces will then produce some resonating cavities that will interact with FBG's reflected signal and degrade its quality. We show in Fig. 1 the different possible reflecting surfaces that the system may have and the main resonating cavities they can produce. The first reflecting surface, M1, is created at the lead fiber output where the refractive index difference generates a typical 4% reflection if air is filling the free-space coupling.
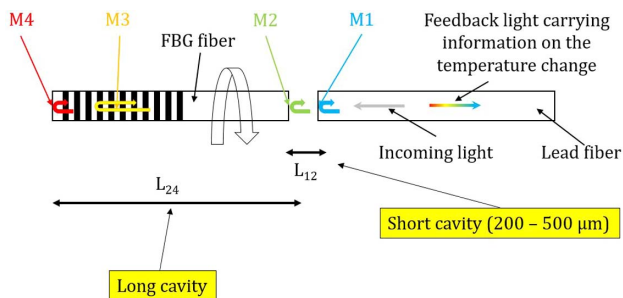

Fig. 1. Reflection sources and the corresponding resonating cavities.

The second reflective surface, M2, is at the FBG fiber entrance inducing a similar reflection than for M1. The third reflecting surface, M3, is the FBG reflection itself and is spectrally limited to the FBG spectral bandwidth. The fourth and last reflection, M4, is located at the FBG fiber end where, most probably, a refractive index change may occur. Then, taking into account the length L_{24} of the FBG fiber that is much longer than the free-space coupling gap, L_{12} ($L_{24} \gg L_{12}$), these length differences generate two main resonating cavities named "long cavity" for the combination of cavity induced by M2 to M3 and M2 to M4, and "short cavity" for M1 to M2.

B. Noise Simulation

Due to the complexity of these resonating effects, a clear view of the resulting signal is difficult to simulate unless an adapted theoretical model is used. For such matter, the well-known matrix theory of multilayer optics is a perfect tool to simulate these noises and analyze their impact on the Bragg wavelength measurement. The multilayer structure can be considered as an optical multilayer stack system with an input and an output that are related with a transfer matrix T. The multilayer stack will be a cascaded system of optical interfaces and layers, each of them having their own transfer matrix to deal with the incident and reflected waves. Figure 2 shows a multilayer stack system example where we can see the electric fields propagating through (forward) and the reflected waves (backward). The incident and refracted wave angles are denoted ϑ_i and ϑ_j, respectively. At each interface, the fields are labeled with the incident layer number with a + or – exponent referring, respectively, to the field located after the interface and before it. Each layer has its complex refractive index n_i and length δ_i.

Then, for a multilayer system, the electric fields at the input and output are related by the transfer matrix of the stack, T_{0N}:

$$\begin{pmatrix} E_F(x_0^-) \\ E_B(x_0^-) \end{pmatrix} = T_{0N} \begin{pmatrix} E_F(x_{N-1}^+) \\ E_B(x_{N-1}^+) \end{pmatrix}. \quad (1)$$

The transfer matrix T_{0N} is composed of the transfer matrices of each multilayer interface and layer. From T_{0N} we can easily retrieve the complete reflection coefficient r:

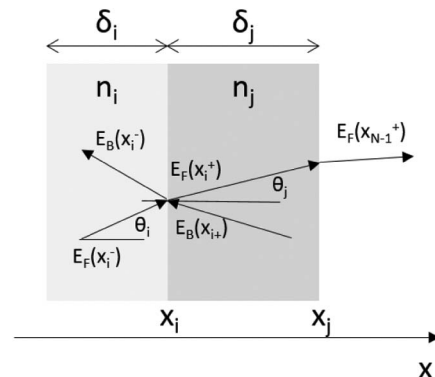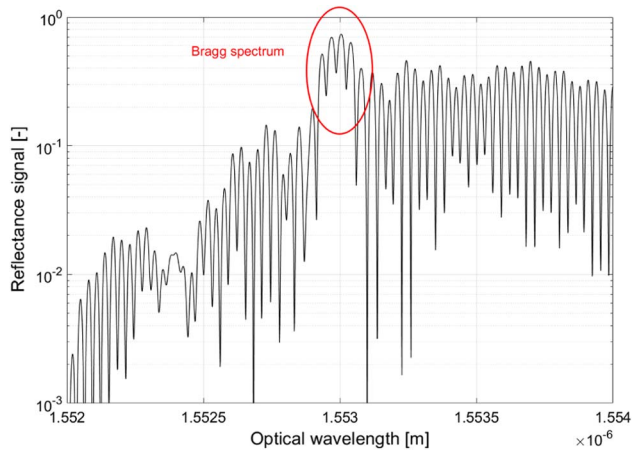$$r = \frac{E_B(x_0^-)}{E_F(x_0^-)} = \frac{T_{21}^{0N}}{T_{11}^{0N}}. \quad (2)$$

Fig. 2. Multilayer stack example with the forward and backward electric fields.

Table 1. Interferometric Noise Simulation Parameters

Resonating Cavities Parts	Length [mm]	RI [−]
Lead fiber	—	1.446
M1 to M2 air cavity	0.6	1
FBG fiber (M2 to Bragg grating)	20	1.446
FBG	5.4	—
FBG low RI	—	1.446
FBG high RI	—	1.44612
FBG fiber (Bragg grating to M3)	2	1.446
RI after M4	—	1

**Fig. 3.** Simulated (3) feedback optical spectrum from a perturbed FBG signal.

This reflection coefficient relates to the input intensity $I_0(\lambda)$ by a simple multiplication and the distorted signal $I_d(\lambda)$ is obtained:

$$I_d(\lambda) = |r|^2 \cdot I_0(\lambda). \tag{3}$$

By using Eq. (3) with the parameters listed in Table 1, we can observe on a logarithmic scale, as shown in Fig. 3, a typical FBG feedback signal perturbed with interferometric noise. The reflectivity of such simulated FBG is almost 80% for a length of 5.4 mm. Basically, the noise has two frequency components: one that is higher than the FBG spectrum itself, which corresponds to the long cavity, and the second one that has a frequency closer to the FBG spectrum and that is induced by the short cavity. The input signal $I_0(\lambda)$ is a laser-like linear ramp whose spectral span is 2 nm and adds a distortion comparable to the low-frequency noise.

C. Noise Impact on the Temperature Measurement
Interrogating a FBG with a current modulated laser induces a redshift of the measured FBG spectrum peak position. This effect is due to a distortion of the FBG spectrum's center of gravity. If the SNR of the FBG is constant, this redshift could, in certain circumstances, be considered as a systematic error that could be easy to compensate. Unfortunately, this SNR will rarely be constant in the presence of low-frequency interferometric noise. This can worsen in the case of a tunable laser whose amplitude is constant in the frequency span, opening
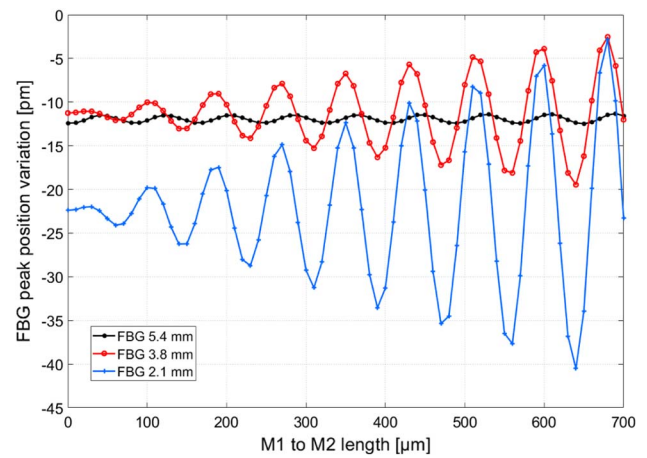
Fig. 4. FBG peak position variation versus M1 to M2 distance for three different FBG reflectivities (FBG length).

the possibilities of a blueshift as well. This blueshift will be induced by a superposition of the FBG peak with a descending portion of the low-frequency interferometric noise. In order to evaluate the influence of this low-frequency interferometric noise on the FBG position, we have again used Eq. (3) and changed the M1 to M2 air cavity length from 0 to 0.7 mm, and for three different FBG's reflectivities (FBG length): 5.4 mm (80%), 3.8 mm (65%), and 2.1 mm (50%). This change of reflectivity has been chosen to simulate a change in the optical coupling between the fibers and then a decreased signal coming from the FBG. For keeping only the interferometric noise effect, the laser input signal $I_0(\lambda)$ has been put equal to 1. The peak position is determined by a classical peak detection using a quadratic fitting after processing a low-pass filter. Results are shown in Fig. 4 and illustrate clearly two phenomena. First, the FBG peak position variations increase when the SNR decreases because its center of gravity is more dependent on the surrounding signal. Second, the FBG peak position variations increase when the M1 to M2 air cavity length increases. This is explained by the fact that, when this length increases, the frequency of this interferometric noise increases and the slope of the noise oscillations is steeper, enhancing the center of gravity distortion effect. Figure 5 shows an effect of this phenomenon with an experimental measurement. In that case, a rotary FBG (Calsens SL), centered at around 1533.7 nm and with a reflectivity of about 65%, is interrogated using a commercial FBG interrogator, Smartscan (Smart Fibres), by linking the FBG and the lead fiber with an optical ferrule (Molex) whose internal diameter is given at 127 μm +3/ − 1 μm. The two fibers are lensed using the lensing configuration of [18]. We can clearly appreciate the FBG position shifting pattern that repeats for every turn due to the air cavity length oscillations and some lateral offset of the fibers outside the optical ferrule that change the FBG SNR. However, the optical ferrule decreases the lateral offset effect but translates it to a longitudinal offset hence changing the phase of the low-frequency interferometric noise that periodically changes the FBG position shift. The order of magnitude of the detected maximum change of the FBG wavelength in Fig. 5 compared
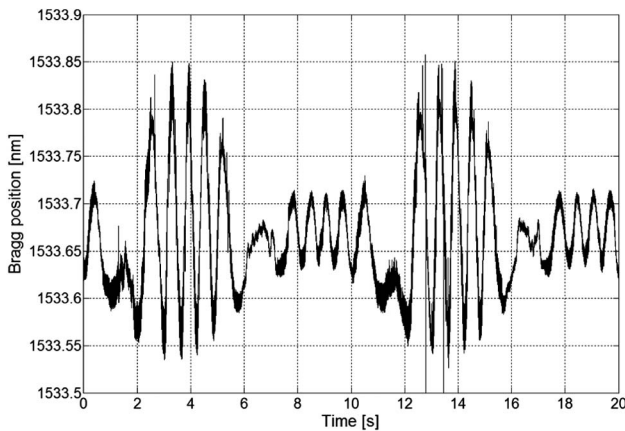
Fig. 5. Rotary FBG (6 rpm) interrogation with a Smartscan interrogator.

to Fig. 4 simulations is explained by the Smartscan working principle. This FBG interrogator has an excellent resolution but this high resolution is achieved through a high-speed scanning sampling rate that allows a massive averaging. Nevertheless, the tunable laser has fixed sampling points spaced of 12.5 GHz for a 40 nm scan. This gives roughly only five points to measure the FBG spectrum. This is clearly not enough to do accurate measurements when in presence of interferometric noise, especially the high-frequency part.

Another aspect of the interferometric noise appears when the rotation stops. Then the FBG position will depend on the specific interaction of the FBG signal with the interferometric noise corresponding at the angular position between fibers. Figure 6 shows that an accurate temperature measurement is impossible to realize if rotation does not occur unless the two fibers are fixed for all measurements and calibrated for this position. Nevertheless, this will never occur for a drill bit application where we aim at measuring the heating of the drill bit while operating it. Hence, a temperature measurement can occur only if the FBG is under rotation so we can average its wavelength position. The FBG wavelength difference observed in Fig. 6 (~0.6 nm) compared to Fig. 5 (~0.3 nm) is essentially due to a non-optimal threshold level detection setting.
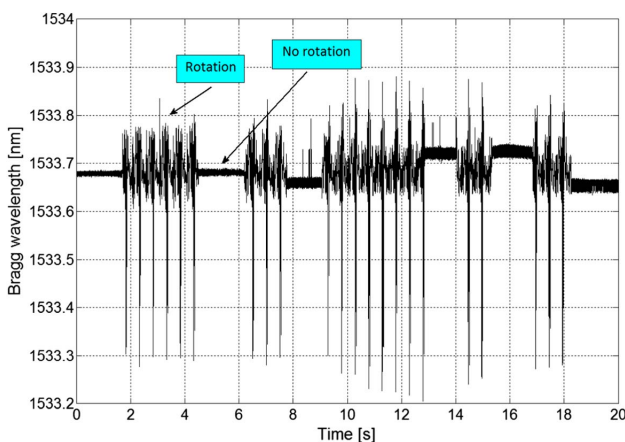

Fig. 6. Interferometric noise effect for rotation stops.

D. Noise Reduction Methods

1. Optical Method

It is clear from Section 2.B that interferometric noise is due to the reflections at the different interfaces. Thus, in order to reduce this interferometric noise, an index of refraction matching is mandatory. This is obtained by using two techniques. The first one is to fill the M1 to M2 gap with an index matching liquid. This method is easily implemented and may potentially be very cost effective. Nevertheless, because of the rotating FBG fiber, some turbulences may appear at the fiber interface, thus increasing the probability of generating air bubbles that would create new resonating cavities. In order to reduce this probability, a liquid flow stronger than the possible turbulences is mandatory. A second technique consists in using anti-reflection (AR) coating on the optical fiber ends. These coatings have the advantage of being able to select the filtering wavelength range or to choose a specific reflection lowering in the surface. However, they can be an expensive solution to implement, especially in applications where the volume of components is small.

In Fig. 7 we can observe the comparison of three different cases of interferometric noise for interrogating the earlier 1533.07 nm centered FBG (Calsens SL). For each case, a lensed lead fiber is aligned to the FBG fiber by using the same optical ferrule as for the Fig. 5 measurements. The FBG fiber is around 100 mm long and the FBG is located at the near end of the fiber (close to M4). The lead fiber and FBG fiber are longitudinally spaced by a 100 μm gap and the FBG fiber is not rotating. The first case shows the result for a lead fiber with no AR coating, Fig. 7(a). We can observe here the low-frequency noise induced by the short cavity M1 to M2 that is characterized by a negative slope on the FBG base spectrum. In the FBG spectrum we can clearly distinguish the high-frequency noise induced by the long cavity M2 to M3. The FBG fiber is 100 mm long, which is roughly 3.5 times the length simulated in Fig. 3 and explains the highest frequency noise we obtain here. The second case uses an AR-coated lead fiber, Fig. 7(b). We can notice here that the low-frequency noise has almost vanished due to the AR coating. Nevertheless, the high-frequency noise still remains as it originates from the M2 to M3 reflections where no AR coating has been applied. The third case, Fig. 7(c), is using the same configuration as for Fig. 7(a) but with water as an index matching liquid to fill the gap between the fibers. We can straightly see the benefits from this action. The two frequency components are significantly diminished and only a small high-frequency noise remains on the FBG useful spectrum. The reflection M4 could be easily eliminated by an angle cleaving, or other means, but as it mainly generates a high-frequency noise outside the FBG spectrum (FBG reflects almost all light within its spectrum band in the cavity M2 to M3), it is useless to decrease it. From these measurements we could conclude that using an index matching liquid would be the best option, but as stated before, the rotation of the FBG fiber will potentially generate air bubbles that will in turn create new resonating cavities. If applied to both fibers, i.e., the lead and FBG fiber, the AR coating will potentially make the two frequency components of the interferometric noise disappear. Unfortunately, in applications where some liquid could infiltrate into the rotary cavity, these
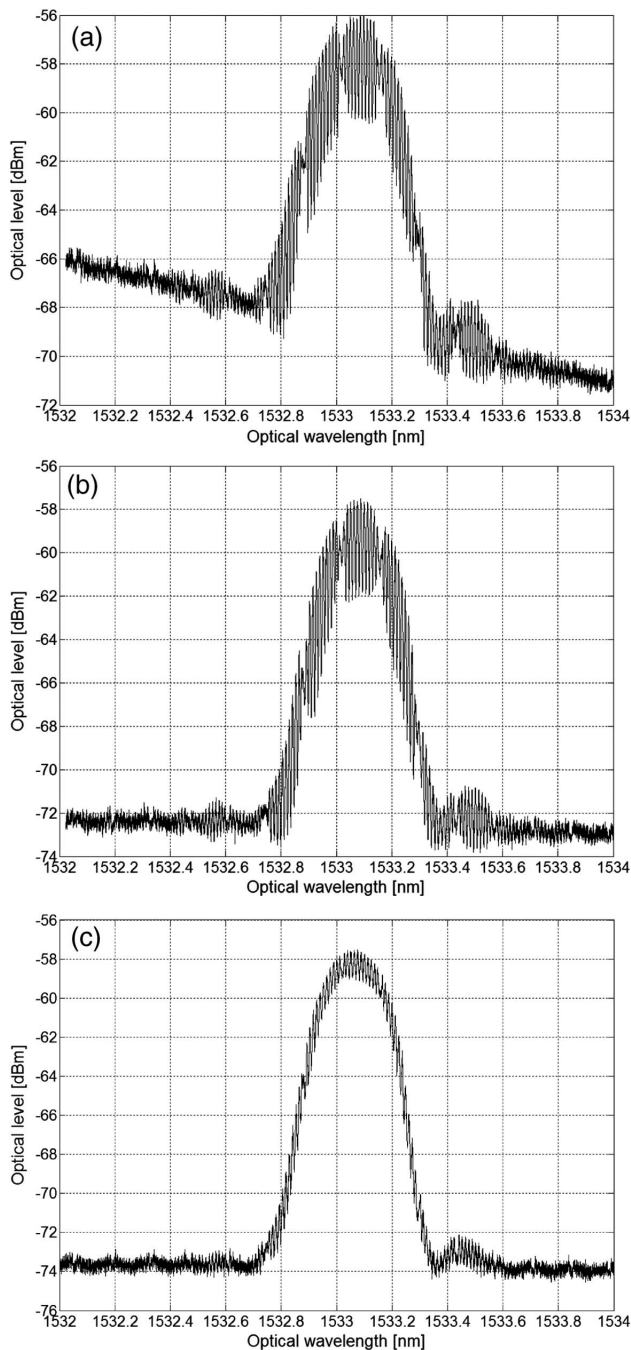
Fig. 8. Signal processing diagram.

FBG feedback signal. This treatment should reduce as much as possible the FBG position errors. The key process here is to adapt an efficient filtering [19] in order to retrieve a clean FBG signal. High-frequency interferometric noise is easily suppressed by a low-pass filter (Fig. 8). The low-frequency noise is unfortunately too close to the FBG signal frequency and hence no filtering process is possible. In our case, the FBG signal can be perceived as being a superposition of a traditional Gaussian-like shaped FBG signal with a positive or negative ramp induced by the low-frequency interferometric noise. It is then necessary to evaluate this ramp and to compensate it in order to retrieve a corrected FBG signal. Finally, a classical peak detection using a quadratic fitting can be used to localize the FBG position.

In order to evaluate the proposed signal processing, a new FBG centered at 1553.07 nm (∼60% reflectivity) has been mounted on a drill tapered for implantology (Nobel Biocare, RP 4.3 × 10 mm) and interrogated with a current swept distributed feedback (DFB) laser (G&H AA1406). The length of the FBG fiber was prepared to be adaptable to an implantology drill bit and was around 30 mm, which is pretty similar to the lengths used for simulations. The fibers have been lensed with a graded-index and spacer configuration (GIS) [20] with a spacer length of 210 μm and graded-index length of 100 μm. These GIS lengths have been optimized by fabricating and testing different spacer and graded-index lengths starting with the Zemax (OpticStudio 18.9) optimal lengths of 250 μm and 100 μm, respectively. The interrogation setup of the FBG was based on the signal processing presented in Fig. 8, and has been implemented on a basic microcontroller (KV5—NXP Semiconductors) without need of a field programmable gate array. The coupling between the lead fiber and the FBG fiber has been realized with an optical ferrule as previously explained in Section 2.C. We can observe in Fig. 9 the spectrum signals before signal processing, after filtering, and after the ramp compensation for two rotary cases (different alignment conditions): a favorable case (a), and a not favorable case (b). We can clearly see that for non-favorable spectra, the processing corrects significantly the measurement error. As a comparison, we can observe the FBG spectrum measured with the Smartscan interrogator in Fig. 10. This measurement shows a spectrum at a favorable case. We can notice that the high-frequency noise starts to be viewable, because of the shortest length of the long cavity, but is not clearly discriminated because of the large laser steps. The filtered and ramp compensated spectrum signal should avoid any measurement error induced by the high-frequency noise and should cancel out the undesired wavelength shift of the FBG position induced by the low-frequency

Fig. 7. Interferometric noise reduction by optical means. (a) Without noise reduction, (b) with AR coating on lead fiber, (c) with water as an index matching liquid.

AR coatings would become useless as, again, air bubbles could appear due to the turbulences of the rotary FBG fiber. Then, for a drill bit application where the presence of coolants is quite common, the use of any of the AR options described above becomes unworkable.

2. Signal Processing Method

As the suppression of the interferometric noise by optical means is practically unfeasible, the option of a proper and efficient signal processing is necessary for the recovery of a
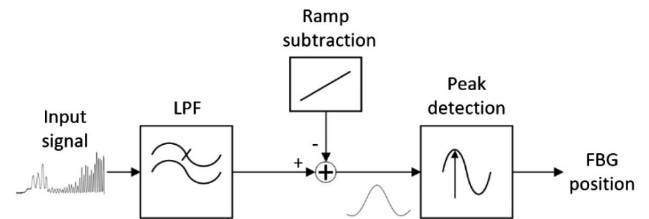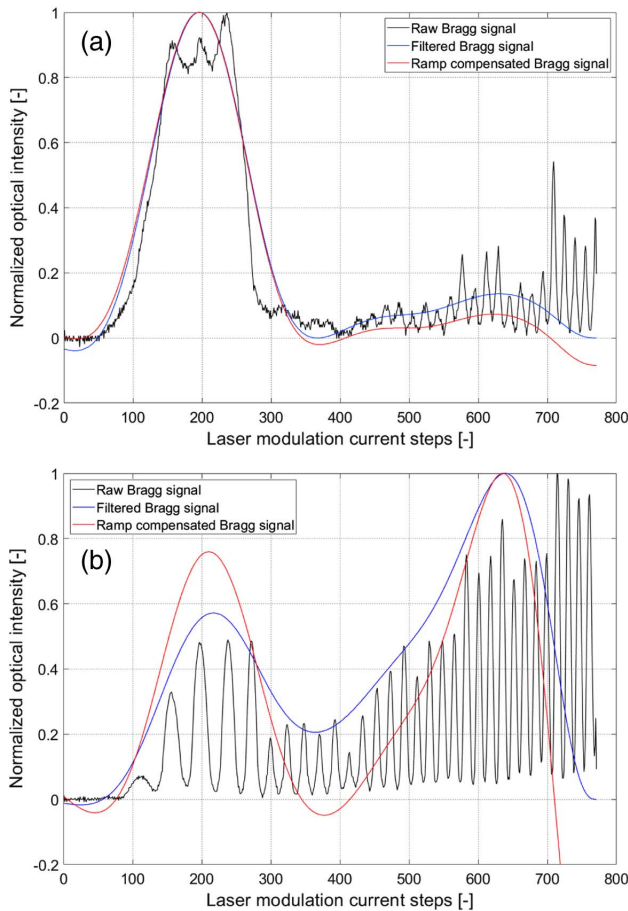
Fig. 9. Spectrum signals before signal processing, after filtering, and after the ramp compensation for two cases: (a) a favorable case, and (b) a not favorable case. The current steps for laser modulation are about 0.18 mA, and starting at 40 mA.

interferometric noise. These are one shot measurements at particular alignment positions and an averaging of the spectrum signals, during rotation, will increase the measurement accuracy, and also avoid the possible signal loss when the Bragg
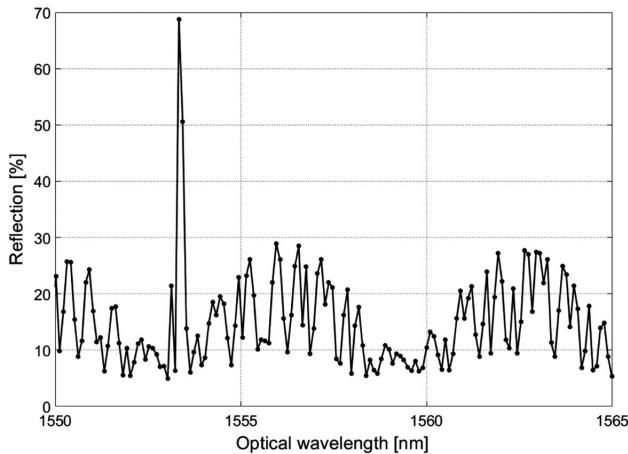

Fig. 10. Optical spectrum, measured with the Smartscan interrogator, of the FBG mounted on an implantology drill bit.

spectrum is not detected due to a too low SNR. We can also notice that on the processed signals a second peak appears on the right-hand side of the measurement. This second peak is due to the filtering of the increasing power coming from the laser as it is positively current modulated with a sawtooth ramp (~0.18 mA per step). The peak detection algorithm is programmed to detect only the first peak corresponding to the FBG signal. The temperature sensitivity of our FBG is around 10 pm/K while our laser source can potentially scan a wavelength span of 2.8 nm. This would give a potential temperature measurement range of 280 K. But obviously, we have to subtract the FBG FWHM two times in order to take into account the ramp extremums giving us a final temperature range of around 230 K for a 30 GHz FWHM FBG.

3. EXPERIMENTAL MEASUREMENTS AND DISCUSSION

For the bone drilling experiments, the drill bit and FBG used in Section 2.D was used together with the electronic processing unit and an adapted dental handpiece (Bien-Air PM 1:1), as it is depicted in the schematic of Fig. 11. Measurements are performed with a sampling rate of 1 ms and then averaged every 100 samples, giving roughly 10 temperature measurements per second. One ramp sample was composed of 1500 points (conversion points/frequency), which is enough to properly discriminate the high-frequency interferometric noise on the FBG spectrum. The FBG was previously calibrated with a thermal bath (Hart Scientific, Model 7025). The performance of heating measurement during drilling is done on a pork jaw sample. Pilot holes with diameters of 2.1 and 3 mm have been prepared. Different measurements are shown in Fig. 12. The first hole is drilled on a pilot hole of 2.1 mm, without cooling. After ~40 s, de-ionized water is sprayed on the drill using a spray water bottle to accelerate its cooling, which explains the sudden dip in temperature (red ring portion on the graph). For the second hole, again, a pilot hole of 2.1 mm is used, but continuous cooling is applied to simulate real-life conditions, but alternate manual squeezing and releasing of the pressure on the water bottle to spray water on the drill induces a non-linear cooling ($t \sim 60$ – 75 s). Finally, a third hole is drilled using the same configuration as for hole 2, but with a pilot hole of 3 mm. Due to a bigger pilot hole diameter, there is less friction and, thus, a lower temperature raise on the drill bit.

These measurements have shown the great potential of FBG for monitoring a drill bit heating during a drilling process.
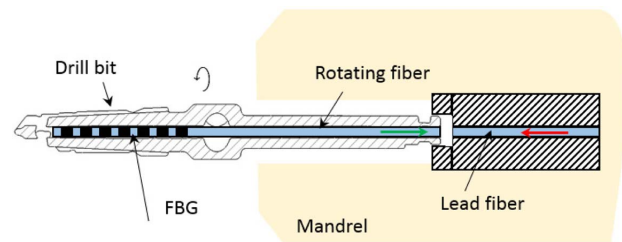

Fig. 11. Schematic of the sensitized implantology drill bit. Red arrow: path of incoming light; green arrow: path of the reflected light from the FBG.
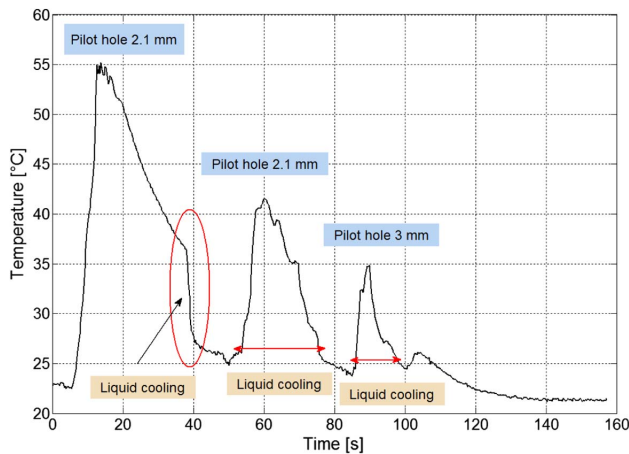
Fig. 12. Temperature measurements on a drill bit during three holes drilling on a pork jaw sample.

The drawbacks induced by the necessity of an optical rotary joint are the generation of an interferometric noise that has mainly two frequency components, and an optical coupling that has to be adapted to ensure an appropriate signal transmission. Interferometric noise is partially filtered out by a low-pass filter while the low-frequency interferometric noise is considered as an additional ramp-like signal that is subtracted from the FBG position signal. The problem of the optical coupling is overcome by lensing the lead fiber and the FBG fiber with a GIS configuration. The miniature size of a standard FBG makes it also an excellent candidate for applications of drill bits of any size and almost any shape. This can be particularly interesting and beneficial for bone drilling where heating control can be a real issue. Nonetheless, the FBG temperature measurement on drill bits is not limited to the bone drilling itself but could be easily adapted to other applications as for metallic drilling or other types of materials.

4. CONCLUSION

In summary, we present a study of a rotary FBG interrogation through a fiber optical rotary joint. The use of a fiber optical rotary joint together with a FBG induces an interferometric noise that complicates seriously an accurate Bragg wavelength interrogation. Thus, we explain the interferometric noise and several ways to overcome it are suggested and evaluated. Finally, a FBG is tested on a commercial implantology drill bit and heating measurements were performed during drilling a pork jaw sample. The results achieved confirmed the great potential of such a kind of optical sensing for the improvement of bone drilling heat monitoring and management.

REFERENCES

1. A. R. Eriksson and T. Albrektsson, "Temperature threshold levels for heat-induced bone tissue injury: a vital-microscopic study in the rabbit," J. Prosthet. Dent. **50**, 101–107 (1983).
2. A. R. Moritz and F. C. Henriques, Jr., "Studies of thermal injury: II. The relative importance of time and surface temperature in the causation of cutaneous burns," Am. J. Pathol. **23**, 695–720 (1947).
3. G. Augustin, S. Davila, K. Mihoci, T. Udiljak, D. S. Vedrina, and A. Antabak, "Thermal osteonecrosis and bone drilling parameters revisited," Arch. Orthop. Trauma Surg. **128**, 71–77 (2008).
4. S. H. Tehemar, "Factors affecting heat generation during implant site preparation: a review of biologic observations and future considerations," Int. J. Oral Maxillofac. Implants **14**, 127–136 (1999).
5. K. Gok, L. Buluc, U. S. Muezzinoglu, and Y. Kisioglu, "Development of a new driller system to prevent the osteonecrosis in orthopedic surgery applications," J. Braz. Soc. Mech. Sci. **37**, 549–558 (2015).
6. G. Augustin, S. Davila, T. Udiljak, D. S. Vedrina, and D. Bagatin, "Determination of spatial distribution of increase in bone temperature during drilling by infrared thermography: preliminary report," Arch. Orthop. Trauma Surg. **129**, 703–709 (2009).
7. R. K. Pandey and S. S. Panda, "Drilling of bone: a comprehensive review," J. Clin. Orthop. Trauma **4**, 15–30 (2013).
8. B. B. Lahiri, S. Bagavathiappan, T. Jayakumar, and J. Philip, "Medical applications of infrared thermography: A review," Infrared Phys. Technol. **55**, 221–235 (2012).
9. E. F. J. Ring and K. Ammer, "The technique of infrared imaging in medicine," Thermol. Int. **10**, 7–14 (2000).
10. M. J. Yacker and M. Klein, "The effect of irrigation on osteotomy depth and bur diameter," Int. J. Oral Maxillofac. Implants **11**, 634–638 (1996).
11. R. Bogue, "Fiber optic sensors: a review of today's applications," Sens. Rev. **31**, 304–309 (2011).
12. É. Pinet, "Fabry-Pérot fiber-optic sensors for physical parameters measurement in challenging conditions," J. Sens. **2009**, 720980 (2009).
13. K. O. Hill and G. Meltz, "Fiber Bragg grating technology fundamentals and overview," J. Lightwave Technol. **15**, 1263–1276 (1997).
14. M. Llera, T. Aellen, J. Hervas, Y. Salvadé, P. Senn, S. Le Floch, and H. Keppner, "Liquid-air based Fabry-Pérot cavity on fiber tip sensor," Opt. Express **24**, 8054–8065 (2016).
15. J. M. Lee and Y. Hwang, "A novel online rotor condition monitoring system using fiber Bragg grating (FBG) sensors and a rotary optical coupler," Meas. Sci. Technol. **19**, 65303 (2008).
16. W. Kim, X. Chen, J. A. Jo, and B. E. Applegate, "Lensless, ultra-wideband fiber optic rotary joint for biomedical applications," Opt. Lett. **41**, 1973–1976 (2016).
17. S. Zilberman, G. Bergovic, E. Shafir, Y. Saadi, O. Mazor, and T. Goichman, "Fiber optic sensing in rapidly rotating structures," Rev. Sci. Instrum. **86**, 115002 (2015).
18. K. H. Tow, M. Llera, S. Le Floch, Y. Salvadé, and L. Thévenaz, "Compact fiber Bragg grating-based thermometer for on-line temperature monitoring of drill bits," Proc. SPIE **9916**, 99162F (2016).
19. C. C. Chan, W. Jin, and M. S. Demokan, "Enhancement of measurement accuracy in fiber Bragg grating sensors by using digital signal processing," Opt. Laser Technol. **31**, 299–307 (1999).
20. Y. Mao, S. Chang, S. Sherif, and C. Flueraru, "Graded-index fiber lens proposed for ultrasmall probes used in biomedical imaging," Appl. Opt. **46**, 5887–5894 (2007).